# A model of cytoplasmically-driven microtubule-based motion in the single-celled *C. elegans* embryo

**Tamar Shinar** [*], **Miyeko Mana** [†], **Fabio Piano** [‡ †] **and Michael Shelley** [*]

[*]Courant Institute of Mathematical Sciences, [‡]Center for Genomics and Systems Biology, and [†]Department of Biology, New York University, New York, NY 10012

Submitted to Proceedings of the National Academy of Sciences of the United States of America

**We present a model of cytoplasmically-driven microtubule-based pronuclear motion in the single-celled *C. elegans* embryo. In this model, a centrosome pair at the male pronucleus initiates stochastic microtubule (MT) growth. These MTs encounter motor proteins, distributed throughout the cytoplasm, that attach and exert a pulling force. The consequent MT-length dependent pulling forces drag the pronucleus through the cytoplasm. On physical grounds, we assume that the motor proteins also exert equal and opposite forces on the surrounding viscous cytoplasm, here modeled as an incompressible Newtonian fluid constrained within an ellipsoidal eggshell. This naturally leads to streaming flows along the MTs. Our computational method is based on an immersed boundary formulation which allows for the simultaneous treatment of fluid flow and the dynamics of structures immersed within. Our simulations demonstrate that the balance of MT pulling forces and viscous nuclear drag is sufficient to move the pronucleus, while simultaneously generating minus-end directed flows along MTs that are similar to the observed movement of yolk granules toward the center of asters. Our simulations show pronuclear migration, and moreover, a robust pronuclear centration and rotation very similar to that observed *in vivo*. We find also that the confinement provided by the eggshell significantly affects the internal dynamics of the cytoplasm, increasing by an order of magnitude the forces necessary to translocate and center the pronucleus.**

pronuclear migration | force generation | microtubules

## Introduction

Proper nuclear migration and positioning are crucial to the successful progression of early development in animal cells and depend on active and passive mechanisms within the cell. In many types of cells, nuclear migration and positioning have been shown to depend on the microtubule (MT) cytoskeleton, and several underlying mechanisms for such MT-based motion have been proposed [1]. One type of MT-based motion occurs in wild type *C. elegans* where the male pronucleus is tightly associated with two centrosomes which act as MT organizing centers (MTOCs) to nucleate MTs. In the sand dollar embryo, it was observed that a male pronucleus associated with an MTOC will move in the direction of the longest MTs until it is centered within the region allowing MT growth [2]. This led to the proposal of cytoplasmically-based length-dependent forces, with the molecular basis being minus-end directed motor proteins such as dynein distributed and anchored in the cytoplasm [2]. Despite the appeal of such a model, one is left to identify the cytoplasmic substrate able to anchor the motor proteins and thus counteract the drag on the MTOC and its associated structures and lead to nuclear motion.

While pronuclear motion under a length-dependent MT-based force model was studied in [3], the nature of the anchoring substrate for motor proteins in the cytoplasm was not considered and forces in the model were not fully balanced. In this work, we present a simple yet mechanically balanced model which yields nuclear motion via MT-based forces actively generated within a viscous cytoplasm. In this model, the cytoplasm is contained within an ellipsoidal shell – the egg periphery – and is modeled as a highly viscous Newtonian fluid. The male pronucleus is a spherical body bound to two MTOCs from which MTs emanate. We include a model of MT growth and shrinkage dynamics where growth is limited by the egg periphery. We use an immersed boundary formulation which allows for the simultaneous treatment of fluid flow and the dynamics of structures immersed within to solve the coupled system (Shinar and Shelley, in preparation). For simplicity, a uniform density of motor proteins in the cytoplasm is assumed, and at each point along an MT filament a motor protein load-velocity relationship is satisfied whereby the *relative local velocity* of the fluid and filament is related to equal and opposite forces acting on the fluid and MT filament, acting in concert with the overall balance of forces within the system. We demonstrate through simulations that this model is sufficient to propel the pronucleus through the viscous cytoplasm while at the same time dragging cytoplasmic fluid particles toward the minus ends of filaments. Here, viscous resistance of the cytoplasmic fluid itself acts as a counterbalance to drag on the pronucleus. We do not model additional anchoring substrates within the cytoplasm, although such structures may be present *in vivo* and could supply greater resistance that would allow for greater absolute motion of the pronucleus.

We demonstrate numerically how the proposed mechanism might contribute to several processes in the single-celled *C. elegans* embryo. Shortly after fertilization, the male pronucleus becomes tightly associated with two centrosomes and migrates from the cell posterior toward the anterior. Simultaneously, the female pronucleus migrates from the anterior toward the male pronucleus, possibly assisted by cortically-driven cytoplasmic flows directed toward the posterior [4]. Pronuclear meeting between the female and male takes place in the posterior of the cell. At meeting, the centrosomes dynamically center between the male and female pronucleus, and the resulting nuclear centrosome complex (NCC) migrates toward the cell center (centration) and rotates 90° to align with the anterior-posterior (AP) axis of the cell (rotation). These events are depicted in Fig. 1A in a live *C. elegans* embryo expressing green flourescent protein (GFP)-tagged $\beta$-tubulin. Our simulations show pronuclear motion such as the early male pronuclear migration, as well as geometry-dependent centration and rotation. Our model also explains the observed fast

**Reserved for Publication Footnotes**

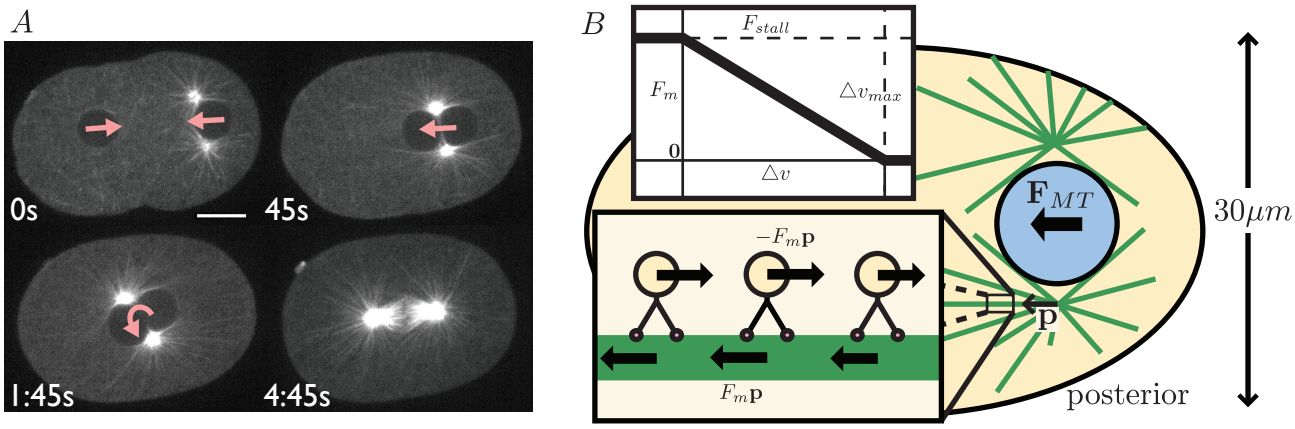


**Fig. 1. A.** MT-based dynamics in a live single-celled *C. elegans* embryo visualized with GFP-tagged $\beta$-tubulin (movie S1). Left to right, top to bottom: migration of the male and female pronuclei, pronuclear meeting, NCC centration, spindle orientation following NCC rotation. Scale bar, $10\mu m$. **B.** Schematic of the biophysical model, with an ellipsoidal cell boundary encapsulating the cytoplasm (yellow), pronucleus (blue) and associated MTs (green). Asymmetric lengths of MTs due to cessation of growth at the cortex creates a force imbalance $\mathbf{F}_{MT}$ favoring centration. Upper inset: The relationship between load $F_m$ and velocity $\triangle v$ for a single motor protein. Lower inset: Motor proteins embedded in the cytoplasm exert equal and opposite forces $\pm F_m\mathbf{p}$ on the cytoplasm and MT filament, resulting in their relative motion.

motion of yolk granules along MT filaments toward the center of asters as the motion of minus-end directed motor proteins under small load. Indeed, the maximum speeds of fast-moving yolk granules of $\sim 1.9\mu m/s$ [5] are very close to measurements of $2\mu m/s$ for the maximum *in vivo* velocity of dynein [6] in early *Drosophila* embryos. While the fast moving yolk granules are visually prominent in live systems, our model predicts that there are also more heavily loaded, slower moving components of the cytoplasm exerting larger forces on MT-bound structures, and that these forces are sufficient for propulsion of pronuclei.

Here we do not model cortically-based active flows, nor asymmetric mechanisms such as those that arise from polarity and play a role in later asymmetric spindle elongation during anaphase [7].

## Biophysical model

The biophysical model is depicted in Fig. 1B. We model the egg periphery as a fixed ellipsoid with a major anterior-posterior (AP) axis of length $50\mu m$ and minor axes of length $30\mu m$. The male pronucleus is modeled as a sphere with radius $R = 5\mu m$. For simplicity, we do not include the female pronucleus, whose motion is influenced by cortically driven cytoplasmic flow [4], as well as by tracking of the astral MTs by motor proteins anchored in the nuclear envelope of the female pronucleus [1]. Note that beyond its early migration away from the posterior, the single pronucleus in the model is taken to represent the NCC after pronuclear meeting. We model the MTs as rigid, one-dimensional rods, rigidly fixed to the pronucleus at the poles of a pronuclear axis initially transverse to the AP axis of the cell.

**Model of cytoplasmic flow and pronucleus.** We model the cytoplasmic medium as an incompressible, viscously dominated, Newtonian fluid. The cytoplasmic velocity, $\mathbf{u}$, and pressure, $q$, then satisfy

$$\nabla \cdot \mathbf{\Sigma} = \mu \triangle \mathbf{u} - \nabla q = -\mathbf{g}_{MT}, \text{ and } \nabla \cdot \mathbf{u} = 0 \qquad [1]$$

where $\mathbf{\Sigma} = -q\mathbf{I} + \mu(\nabla \mathbf{u} + \nabla \mathbf{u}^T)$ is the stress tensor for a Newtonian fluid and $\mu$ is the viscosity. Here, $\mathbf{g}_{MT}$ is the MT-based force density (Eq. 4) that drives the flow. Assuming a Newtonian fluid response agrees with [8], where extent and time lag of mean squared displacements of nanoparticles were measured *in vivo* to infer viscoelastic properties of the cell. Results indicated that during the single-cell stage, the cytoplasm behaves like a liquid with a spatially and temporally uniform high viscosity of approximately 10 poise (water at 20°C has a viscosity of approximately 1 centipoise) and negligible elasticity. Note that using nanoparticles may bias results toward a Newtonian interpretation [9]. Inertial effects in the cytoplasm are ignored as is appropriate here (the Reynolds number is approximately $10^{-5}$). We also ignore thermal fluctuations in the fluid.

The egg periphery is assumed to be of fixed shape and the no-slip boundary condition is applied there. This ignores cortical motions investigated by others [10]. The pronucleus is assumed to be a solid body moving under rigid body translation and rotation. A no-slip condition matches the fluid velocity at the boundary of the pronucleus to that of the translating and rotating body with rigid body velocity $\mathbf{V}$ and angular velocity $\mathbf{\Omega}$. Without any applied force, the pronucleus remains stationary. Here, the applied force arises from the action of motor protein pulling forces acting on the attached MTs. The consequent force, $\mathbf{F}_{MT}$, and torque, $\mathbf{T}_{MT}$, on the pronucleus due to the MT forces is balanced by the total fluid force and torque on the pronucleus:

$$\begin{pmatrix} \mathbf{F}_{MT} \\ \mathbf{T}_{MT} \end{pmatrix} + \begin{pmatrix} \int_{\partial B} \mathbf{\Sigma} \cdot \mathbf{n}\, dS \\ \int_{\partial B} \mathbf{r} \times \mathbf{\Sigma} \cdot \mathbf{n}\, dS \end{pmatrix} = \mathbf{0}, \qquad [2]$$

where $\partial B$ is the surface of the pronucleus, with $\mathbf{n}$ its outward unit normal and $\mathbf{r}$ its position relative to the center of mass of the pronucleus. Given $\mathbf{F}_{MT}$ and $\mathbf{T}_{MT}$, solution of the Stokes equations (1) under these boundary conditions and force balances (2) yields $\mathbf{V}$ and $\mathbf{\Omega}$. However, $\mathbf{F}_{MT}$ and $\mathbf{T}_{MT}$ must themselves be determined as part of the dynamics problem. We do not include the effect of fluid drag on the MTs in these computations.

**Microtubule dynamic instability.** The MTs are polar structures with their minus ends anchored in the centrosome and plus ends emanating radially out from the centrosome (see Fig. 1B). The growth and shrinkage of MTs due to polymerization and depolymerization of their constituent tubulin dimers is described by the model of dynamic instability [11].

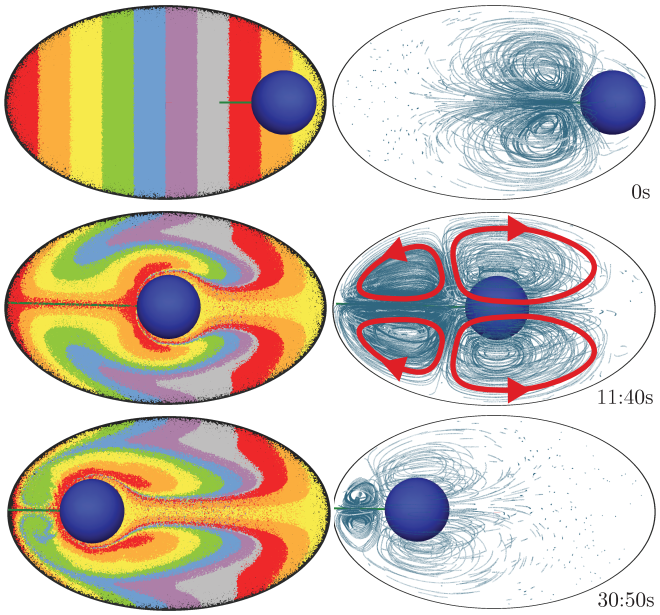


**Fig. 2.** Frames from the simulation of a simple example demonstrating the propulsion mechanism (movie S3). A slice through the three-dimensional volume is shown. A filament is pulled along its length by motor proteins embedded in the cytoplasm. The attached pronucleus moves toward the anterior while the cytoplasm along the filament moves to the posterior. Left column: colored passive tracer particles have been added for visualization. Right column: streamlines of the flow. The flow structure consists of two toroidal vortices, one centered at the filament and one centered at the pronucleus.

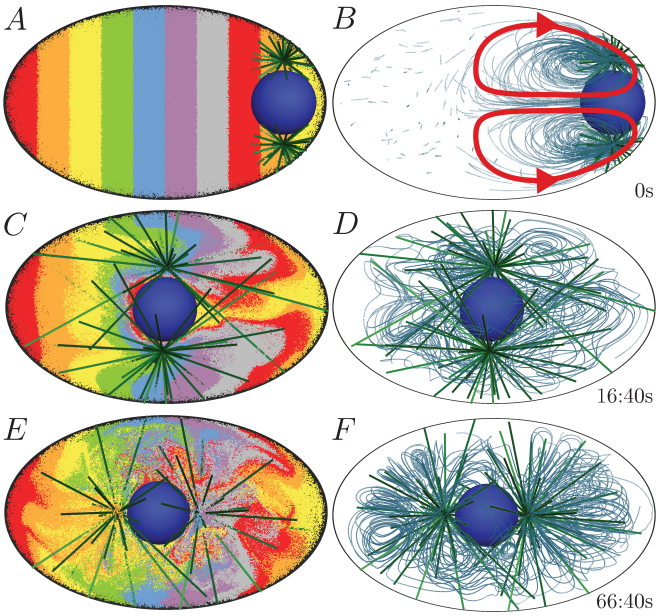


**Fig. 3.** Frames from the simulation of the full WT model (movie S4). A slice through the three-dimensional volume is shown. The NCC starts at the posterior (top row). Asymmetric lengths of MTs due to cessation of MT growth at the cortex leads to centration of the NCC (middle row). Fluctuations in the MT lengths initiate a rotation of the NCC which continues until it is aligned with the AP axis (bottom row). Left column: colored passive tracer particles have been added for visualization. Right column: streamlines of the flow.

As in [3],[12], we use a simple version of this model specified by four constant parameters: the growth velocity, shrinkage velocity, catastrophe frequency and rescue frequency. The transition of an MT from growth to shrinkage (shrinkage to growth) is described by a Poisson process with rate parameter equal to the catastrophe (rescue) frequency; See [13] for a detailed description. MTs that would otherwise extend beyond the cell boundary are shortened so that their plus ends lie on the boundary.

**Pulling force model.** In the present model, minus-end directed motor proteins move along the length of polar MT tracks, transporting cargo while exerting a pulling force on the MT and its associated structures. Our model is based on the models described in [3] and [12], with the important difference that we locally model the interaction of the active fluid and the filament, and can thus model the relationship between motor protein load and local relative velocity of the motor protein and filament. Because the pulling is actuated along the lengths of filaments (as opposed to, e.g., special sites at the cortex), the resulting forces are length-dependent. Consequently, the NCC will assume a favored position and orientation within the cell. This is discussed further below.

The force density at distance $s$ along the MT is given by

$$\mathbf{G}_{MT}(s) = D(s)F_m(s)\mathbf{p},$$

where $D(s)$ is the density per unit length of motor proteins, $F_m$ is the force exerted on the MT by a single motor protein, and $\mathbf{p}$ is the direction vector for the MT. We take $D(s)$ to be constant. The force $F_m$ is given by

$$F_m(s) = F_{stall}\left(1 - \frac{\widehat{\triangle v}(s)}{\triangle v_{max}}\right),$$

where $\widehat{\triangle v}(s) = \min(\max(\triangle v(s), 0), \triangle v_{max})$ and $\triangle v(s)$ is the relative velocity of the MT and the motor protein at $s$ projected onto the direction $\mathbf{p}$ (see plot in Fig. 1B). An expression of this form was used in [3], but there the velocity was the absolute velocity of the MT, yielding a different value of $F_m$ (especially where fluid is fast moving) and hence different dynamics. The force and torque exerted by an MT on the associated pronucleus is given by

$$\begin{pmatrix} \mathbf{F}_{MT} \\ \mathbf{T}_{MT} \end{pmatrix} = \begin{pmatrix} \int_C \mathbf{G}_{MT}(s)\, ds \\ \int_C \mathbf{r}_{MT}(s) \times \mathbf{G}_{MT}(s)\, ds \end{pmatrix} \qquad [3]$$

where $C$ represents the one-dimensional MT with position $\mathbf{X}_{MT}(s)$, anchored in a centrosome at $s = 0$ and of length $L$, and $\mathbf{r}_{MT}(s) = \mathbf{X}_{MT}(s) - \mathbf{X}_0$ is position on $C$ relative to the center of mass $\mathbf{X}_0$ of the pronucleus. To express the equal and opposite force on the fluid due to the motor proteins, the Lagrangian force density $\mathbf{G}_{MT}$ is converted to an Eulerian force density $\mathbf{g}_{MT}$ through the relation (see [14])

$$\mathbf{g}_{MT}(\mathbf{x}, t) = -\int_C \mathbf{G}_{MT}(s)\delta(\mathbf{x} - \mathbf{X}_{MT}(s,t))\, ds, . \qquad [4]$$

**Parameters in the biophysical model.** Parameters in the model include the cytoplasmic viscosity $\mu$, the number of MTs associated with each centrosome, the MT growth and shrinkage velocities and rescue and catastrophe frequencies, motor protein stall force, and maximum motor protein velocity. We use the parameter values given as the standard condition in [3], Table 1. See [3] and the references therein for the sources of these parameters. Note that [3] tuned the motor protein density parameter $D$ so that centration occurred at observed time scales. We did not tune parameters. Force magnitudes increase linearly with $D$ and hence we expect velocities to increase and timescales to decrease linearly with $D$ as well. Thus, such quantities in the results are meaningful in relative

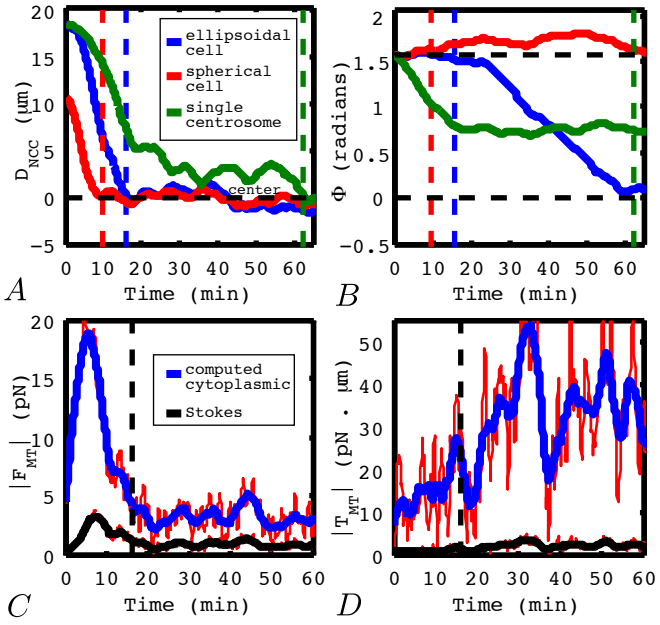


**Fig. 4. A.** Position of NCC along AP axis. **B.** Angle of NCC to AP axis. The vertical dashed line indicates the time of centration. **C.** Net cytoplasmic drag force computed in the present model (accounting for the enclosing geometry of the cell) compared with the drag estimated by Stokes' Law (which assumes an open geometry). **D.** Net cytoplasmic torque computed in the present model (accounting for the enclosing geometry of the cell) compared with the torque estimated by Stokes' Law (which assumes an open geometry). Red lines are the raw data, and the blue and black lines are moving averages, shown for clarity.

terms only. Similar to [3], we find the qualitative aspects of the motion to be robust to variations in the parameter values.

## Results

**Pronuclear translation and cytoplasmic flow due to a bundled, parallel array of filaments.** To begin, we study a much simplified configuration of our model that illustrates that the pronucleus can be propelled by pulling directly on the viscous cytoplasm and that a counterflow of cytoplasm is generated (Fig. 2). We emphasize that we are not modeling any additional structures in the cytoplasm. A pronucleus located at the posterior is attached to a bundle of ten parallel filaments (represented in the model by a single filament with a force multiplier of ten) directed toward the anterior and oriented along the AP axis. From a three-dimensional simulation of this model, Fig. 2 shows how cytoplasmic material is displaced, and the associated flow structures (movie available as supporting material S3). Under the action of cytoplasmic pulling on the growing MT bundle, the pronucleus translates toward the anterior, while cytoplasm is pulled along the MT bundle towards the posterior. Flow streamlines show the appearance of two toroidal vortices, one about the MT and the other about the nucleus. This flow structure is associated with a "puller" type microswimmer (see [15]) as the tangential active stresses along the MT create fluid slip along the filament, while cytoplasm is dragged with the body due to the no-slip condition. While this simple model illustrates nicely how cytoplasmic pulling can translate the nucleus, the models lacks a proper balance of MT-induced pulling forces. Hence, the nucleus overshoots the center, and shows neither centration nor subsequent rotation at the center for proper positioning.

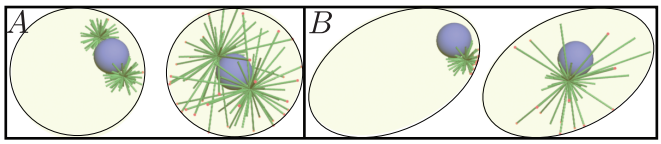


**Fig. 5. A.** The initial and final configuration for a spherical embryo. The NCC centers but fails to rotate. **B.** The intial and final configuration for an embryo with a single centrosome (movie S6). NCC positioning and orientation are disrupted.

**Centration of the nuclear centrosome complex.** We now simulate our full three-dimensional model of NCC motion under cytoplasmically-driven MT-based pulling forces. This model of wild type (WT) embryo assumes an ellipsoidal periphery containing a spherical NCC with two MTOCs located at poles whose axis is initially tranverse to the AP axis. Figure 3A shows the two MT arrays shortly after growth is initiated while Fig. 3B shows the early-time flow structure set up by cytoplasmic pulling. MTs that reach the cell periphery are prevented from growing further. Thus, by the NCC being initially at the posterior, MTs grow preferentially towards the anterior and this anterior-posterior length imbalance drives centration. Fig. 4A (blue) plots the evolution of NCC position $D_{NCC}(t)$ along the AP axis, with 0 indicating the cell center, showing that the NCC stops migrating upon reaching the center but remains subject to random perturbations due to the stochastic dynamics of the MTs. Figures 3C and D show that the flows associated with the MT array are very complex, with continual cytoplasmic streaming along MTs towards the centrosomes (see supporting material S4).

**Rotation of the nuclear centrosome complex.** While the NCC is stably positioned at the cell center, it is unstable to rotation away from the centrosomal axis being transverse to the AP axis. Random fluctuations in orientation provide the perturbations that again lead to an imbalance in MT length, though in case for MTs that are exerting forces tangential to the NCC. This yields a developing rotational torque. Consequently, the NCC undergoes a 90° rotation as it nears the center and assumes a stable orientation aligned with the AP axis as seen in Fig. 3E and F. Figure 4B (blue; dashed vertical lines indicate time of centration) plots the evolution of the angle $\Phi(t)$ between the inter-MTOC axis and the AP axis; The NCC begins slowly rotating somewhat before centration and continues until it is aligned with the AP axis.

Such centering and rotation is a consequence of the length-dependence of the forces and the geometry of the cell. In particular, a full model of the fluid is not required to see these qualitative effects, and they were also demonstrated with the simpler model of [3] in a subsequent work by the same authors [16].

**The confining geometry of the ellipsoidal cell increases the necessary pulling forces.** We now consider the forces and torques associated with centration and rotation. Figures 4C and D show the total force and torque (green curves) exerted upon the NCC by MT-based pulling forces, which is exactly balanced and opposed by fluid drag upon the NCC (Eq. 2). In the epoch leading up to centration, the rise of total force is associated with the MT-length imbalance initiated by MT growth. The length imbalance disappears as the NCC centers and the total force drops. The total torque grows up to and through centration and is associated with the rotation of the NCC centrosomal axis towards alignment with the AP axis.

In [3], male pronuclear migration was studied under both cortical pushing and length-dependent cytoplasmic pulling

force models against cytoplasm whose drag was modeled using Stokes' Law. Stokes' Law follows from computing the motion of a sphere in an infinite fluid with no boundaries. However, for viscous flow, the presence of a confining geometry such as that of the eggshell has a significant impact on both the magnitude of viscous drag forces and on the resulting flow structure. By including a flow model for the cytoplasm, we can more accurately compute the dynamics of the system. Fig. 4C also shows drag force estimate based on the instantaneous velocity using Stokes' Law $\mathbf{F}_d = 6\pi\mu R\mathbf{V}$ (black curve). Note that the Stokes' drag corresponding to the motion is significantly smaller than the computed drag. Similarly, the computed cytoplasmic torque on the nuclear body is significantly larger than the Stokes' Law estimate given by $\mathbf{T}_d = -8\pi\mu R^3\mathbf{\Omega}$.

**Two perturbations of the model.** We now consider two interesting perturbations from the full WT model. In the first, the ellipsoidal periphery is replaced by a spherical one of the same volume, corresponding to an embryo with its shell removed as studied in [7]. In the second, we model NCC motion, again in the ellipsoidal geometry, but with only one centrosome corresponding to a *zyg-1* mutant where centrosome duplication fails [17],[3]. The NCC dynamics of these two cases is shown in Figs. 5A and B, respectively (see also S5 and S6 for supporting video).

In both cases the NCC sits initially at the posterior and MT growth is biased towards the interior of the cell. This again leads to migration towards the center. In the spherical periphery case this yields stable centration, though the rate of initial displacement from the periphery is steeper than in the ellipsoidal cases; see Fig. 4A). The is due to the fact that the spherical boundary is flatter than the ellipsoidal boundary near NCC initial position, making it easier to draw in cytoplasmic fluid behind the NCC as it moves away from the posterior. In the single centrosome case, the MTOC approaches the cell center (where $D_{NCC} \approx 3.5\mu m$) on a time scale comparable to that in the WT case (Fig. 4A (green)), despite the NCC having 50% fewer force-generating MTs. This is because competing pulling forces toward the posterior are reduced as the NCC rotates toward the anterior. Note, however, that positioning of the NCC is significantly affected and is more sensitive to MT fluctuations.

In the spherical case, no particular orientation is favorable over another and so the NCC angle exhibits random drift from its initial value (Fig. 4B (red)). In the single centrosome case, the initial force imbalance between the two poles of the nucleus is large due to the absence of one MTOC, and thus the NCC begins rotation immediately as the single MTOC is pulled toward the center of the cell; see Fig. 4B (green). However, this rotation does not lead to proper alignment with the AP axis, but rather the NCC angle approaches some intermediate value near $\pi/4$.

## Discussion

**Pulling on microtubules by cytoplasmic components.** Cytoplasmically-driven MT-based forces have been previously considered as a possible mechanism for nuclear and spindle positioning [2], [1]. In such a model, minus-end directed motor proteins distributed throughout and anchored in the cytoplasm exert length-dependent pulling forces on MT filaments resulting in motion of MT-bound structures. A length-dependent pulling force model was studied in [3], where the authors concluded that qualitative aspects of the male pronuclear migration *in vivo* were consistent with the

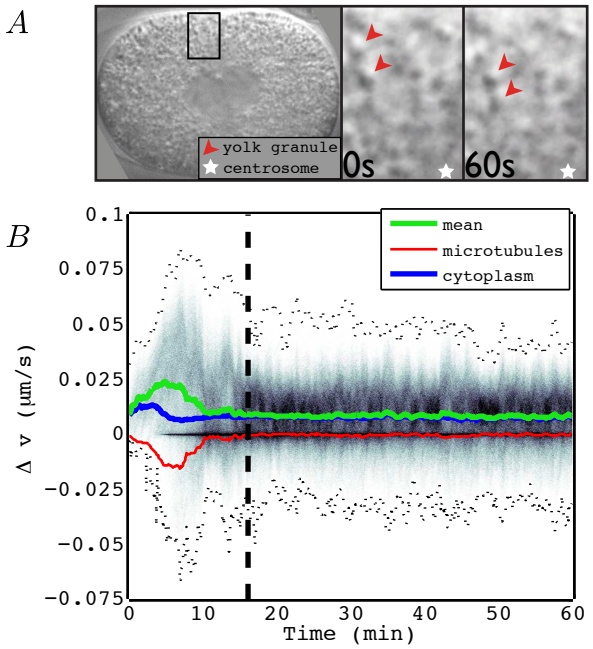


**Fig. 6. A.** Linear motion of yolk granules along the length of MT filaments toward the centrosome is evident in a DIC movie of a live embryo (movie S2). **B.** The background density shows the distribution of motor protein velocities along the lengths of MTs throughout the simulation of the WT case, with its mean (green) and boundaries (dotted lines). The mean MT velocity (red) and cytoplasm velocity (blue) along MTs, directed toward minus ends, are also shown.

length-dependent pulling mechanism rather than a pushing mechanism. However, an anchoring substrate for motor proteins in the cytoplasm has not been demonstrated, though structures such as the actin cytoskeleton and endoplasmic reticulum have been suggested (see [18], Box 1).

We assume that the motion of a motor protein along an MT creates a minus-end directed force in the fluid, perhaps by the motor protein carrying a payload. We assume also a constant and uniform distribution of minus-end directed motor proteins, which more generally represents the balance of minus-end directed motors over opposing mechanisms such as plus-end directed motors. In *C. elegans*, dynein is present throughout the cytoplasm in a punctate manner during the first cell division [5].

A set of experiments in sand dollar eggs provides direct evidence for cytoplasmically-driven forces driving pronuclear motions. In [2], eggs were treated with the MT depolymerizing drug colcemid. The effect of the drug was then selectively inhibited through spatially controlled and localized UV irradiation. When a circular region containing the sperm aster, but not the female pronucleus nor the cortex, was irradiated, the sperm aster migrated in the direction of its longest MTs until it centered within the irradiated region. This demonstrated that MT contact with the cortex was unnecessary for male pronucleus motion. These experiments suggest that the pronuclear motion was MT-based and driven by components in the cytoplasm. Futhermore, the force mechanism resulted in centering within a circular region.

Fast movement of yolk granules toward the centers of asters has been observed in the sand dollar [2] and in *C. elegans* [5]. This is shown in Fig. 6A, where two yolk granules moving toward the centrosome are indicated at two points along their trajectories. Dynein was shown to be responsible for similar motion of lipid droplets along MT filaments in

early *Drosophila* embryos [6]. Such movement indicates the presence of cytoplasmic pulling forces on MT filaments. A motor protein moving under negligible load exhibits fast motion while one moving under signficiant load exhibits slow motion (Fig. 1B, upper inset). A yolk granule under small load in turn exerts a small pulling force on the MT. A similar yolk granule subject to larger drag due to interactions with surrounding cytoplasm would in turn exert a larger pulling force on the MT. Such a yolk granule would not be visually prominent as it would not be fast-moving. Our model both explains the fast movement of yolk granules, and predicts that slower moving, more highly loaded cytoplasmic components can generate sufficient force to position the pronuclei. The average speeds of experimentally observed fast-moving yolk granules in anaphase were plotted in [5], Fig. 3B. The maximum granule speeds of $\sim 1.9\mu m/s$ are very close to measurements of $2\mu m/s$ for the maximum *in vivo* velocity of dynein reported in [6]. In analogy to that figure, in Fig. 6B we plot *all* velocities along MTs throughout the simulation, because we know precisely where MTs are at any time in the simulation, we can measure velocities everywhere along MTs, even where the fluid is moving slowly. The plot shows that on average, motor proteins and cytoplasm move along MTs toward minus ends, while MTs move toward plus ends. The spike in density of motor protein velocities near zero occurs close to the pronuclear body, because cytoplasm cannot flow freely into the centers of MTOCs due to incompressibility.

**Additional mechanisms for nuclear and spindle positioning.** Several additional mechanisms for nuclear and spindle positioning have been proposed (see reviews in [1] and [18]), and we briefly discuss these here.

Pushing forces due to polymerization of MT filaments against a resisting barrier have been investigated as a possible mechanism of male pronuclear migration. This mechanism was investigated in [3] and found to be less signficiant than a pulling mechanism. It was also noted in [5] that the male pronucleus fails to move away from cortex in dynein heavy chain *dhc-1* mutants, although the mechanisms underlying the pushing model were presumably intact.

There is evidence that direct pulling between the male and female pronuclei plays a significant role in pronuclear motion up to pronuclear meeting. In the colcemid/UV experiments of [2], male pronuclear migration was 2-4 times faster when the female pronucleus was in the irradiated region than when it was outside the region, and the female pronucleus also migrated in this case. Plots of male and female pronuclei position vs. time in sand dollar ([2], Fig. 7) and *C. elegans* ([19], Fig. 3) show an acceleration of the motion as the bodies approach one another, possibly due to their association through a larger number of MT filaments interacting with the nuclear envelopes, where dynein is enriched [5].

The prevailing model for spindle positioning appears to be cortically driven pulling forces [20], where cortical force generators are balanced during symmetric positioning and unbalanced during asymmetric positioning, and control of positioning is achieved through regulation of cortical force generators. Possible mechanisms include capture and depolymerization of MTs at special sites on the cortex [21], as well as actin-based translocation of MTs along the cortex.

While the above mechanisms are likely involved in nuclear and spindle positioning, they cannot be fully responsible for the phenomenon demonstrated in [2], as the areas of UV radiation were spatially isolated from the cortex in those experiments. Furthermore, unlike the cytoplasmically-based model, these models do not predict the observed movement of yolk granules toward the center of asters.

**Geometry-dependence of microtubule-based forces in the centering and rotation of the NCC.** Following pronuclear meeting, the NCC migrates to the center of the ellipsoidal cell and rotates 90° so that the spindle is aligned with the AP axis [22]. While spindle position and orientation in the single-cell *C. elegans* embryo have been shown to be coupled to polarity cues (for a recent review see [23]), experiments interfering with such cues demonstrate geometry-dependent spindle positioning and orientation [7].

In the pulling model, minus-end directed motor proteins are assumed to be uniformly distributed and anchored throughout the cytoplasm. Therefore, a longer MT can associate with more motor proteins, resulting in a force that is directly proportional to the MT length. When the NCC is offset from the center of the cell an MT length imbalance favoring the direction of the cell center develops, and the net MT-based force on the NCC is directed toward the the cell center (see Fig. 1B). Our simulations reproduce this centering within a symmetric geometry, as depicted in Fig. 3. The NCC position is stable in the cell center under the present model, and once in the cell center, it undergoes only small fluctuations due to randomness in the MT forces.

In our simulations, we observed that the NCC began to passively rotate as it approached the cell center and once centered continued to rotate until it aligned with the AP axis (Fig. 4B). That orientation was stable to continuing perturbations due to fluctuations in MT forces. The passive rotation results from symmetry breaking in the geometric positioning or orientation of the NCC, which in the cell could be due to a number of factors such as constitutive variations within the cell, the dynamics of the finite number of MTs, etc.

In the spherical case we simulated, rotation failed due to the absence of any orientational asymmetries in the forces. Experimentally, rotation is observed in otherwise unaltered spherical embryos [24], [7]. However, this observed rotation was shown to depend on molecular mechanisms acting downstream of the *par* proteins [7]. In *par-3* mutants, rotation in spherical embryos failed, while in normally shaped oblong *par-3* mutant embryos, rotation was observed [7]. Thus polarity related molecular mechanisms in the cell appear to induce geometric asymmetries even in the absence of extrinsic geometric asymmetries. Since we do not model polarity in the cell, our results concerning rotation of the NCC are more consistent with embryos where polarity is disrupted. Interestingly, it was also noted in [24] that actin microfilaments may be required for rotation to occur in the spherical geometry whereas they may not be required in the ellipsoidal geometry.

## Conclusion

We have presented a simplified model of MT-based motion transduced through interaction of MT filaments with active elements in the cytoplasm. We have demonstrated the feasibility of pronuclear and NCC motion through direct interaction with active elements in the cytoplasm along the length of MTs without assuming the presence of additional structures for anchoring motor proteins. We have illustrated that geometry-dependent centration and rotation can result passively as a consequence of the MT force model and the cell shape. We have shown that the inclusion of the cytoplasmic hydrodynamics in simulations of pronuclear migration significantly affects the cytoplasmic drag forces on the pronucleus. When filaments are aligned in parallel, this process can generate strong cytoplasmic flows, as illustrated in the simplified, bundled filament example. Thus, this model is applicable to other phenomena, for example, cytoplasmic streaming in other organisms and axonal transport of organelles. More

generally, it is applicable to the interaction of motor proteins and polar filaments within a fluidic environment.

**ACKNOWLEDGMENTS.** We would like to thank Kris Gunsalus and Charlie Peskin for helpful discussions. Grants. KITP.

1. Reinsch S, Gönczy P (1998) Mechanisms of nuclear positioning. Journal of Cell Science 111:2283–2295.
2. Hamaguchi MS, Hiramoto Y (1986) Analysis of the role of astral rays in pronuclear migration by the colcemid-uv method. Dev. Growth Differ. 28:143–156.
3. Kimura A, Onami S (2005) Computer simulations and image processing reveal length-dependent pulling force as the primary mechanism for C. elegans male pronuclear migration. Developmental Cell 8:765–775.
4. Hird SN, White JG (1993) Cortical and cytoplasmic flow polarity in early embryonic cells of Caenorhabditis elegans. The Journal of Cell Biology 121:1343–1355.
5. Gönczy P, Pichler S, Krikham M, Hyman AA (1999) Cytoplasmic dynein is required for distinct aspects of mtoc positioning, including centrosome separation, in the one cell stage Caenorhabditis embryo. The Journal of Cell Biology 147:135–150.
6. Gross SP, Welte MA, Block SM, Wieschaus EF (2000) Dynein-mediated cargo transport in vivo. a switch controls travel distance. The Journal of cell biology 148:945–956.
7. Tsou MB, Hayashi A, DeBella LR, McGrath G, Rose LS (2002) LET-99 determines spindle position and is asymmetrically enriched in response to PAR polarity cues in C. elegans embryos. Development 129:4469–4481.
8. Daniels BR, Masi BC, Wirtz D (2006) Probing single-cell micromechanics in vivo: The microrheology of C. elegans developing embryos. Biophysical Journal 90:4712–4719.
9. Valentine M, Perlman Z, Mitchison T, Weitz D (2005) Mechanical Properties of Xenopus Egg Cytoplasmic Extracts. Biophysical Journal 88:680–689.
10. Mayer M, Depken M, Bois JS, Jülicher F, Grill SW (2010) Anisotropies in cortical tension reveal the physical basis of polarizing cortical flows. Nature 467:617–621.
11. Mitchison T, Kirschner M (1984) Dynamic instability of microtubule growth. Nature 312:237 – 242.
12. Nédélec F (2002) Computer simulations reveal motor properties generating stable antiparallel microtubule interactions. The Journal of Cell Biology 158:1005–1015.
13. Desai A, Mitchison TJ (1997) Microtubule polymerization dynamics. Annu. Rev. Cell Dev. Biol. 13:83–117.
14. Peskin C (2002) The immersed boundary method. Acta Numerica 11:479–517.
15. Saintillan D, Shelley MJ (2007) Orientational Order and Instabilities in Suspensions of Self-Locomoting Rods. Physical Review Letters 99:058102+.
16. Kimura A, Onami S (2007) Local cortical pulling-force repression switches centrosomal centration and posterior displacement in c. elegans. The Journal of Cell Biology 179:1347–1354.
17. O'Connell KF, et al. (2001) The C. elegans zyg-1 Gene Encodes a Regulator of Centrosome Duplication with Distinct Maternal and Paternal Roles in the Embryo. Cell 105:547–558.
18. Goñczy P (2002) Mechanisms of spindle positioning: focus on flies and worms. Trends in Cell Biology 12:332–339.
19. Albertson D (1984) Formation of the first cleavage spindle in nematode embryos. Developmental Biology 101:61–72.
20. Grill S, Hyman A (2005) Spindle positioning by cortical pulling forces. Developmental Cell 8:461–465.
21. Howard J, Hyman AA (2003) Dynamics and mechanics of the microtubule plus end. Nature 422:753–758.
22. Oegema K, Hyman AA (2006) Cell division. WormBook.
23. Siller KH, Doe CQ (2009) Spindle orientation during asymmetric cell division. Nat Cell Biol 11:365–374.
24. Hyman AA, White JG (1987) Determination of cell division axes in the early embryogenesis of Caenorhabditis elegans. The Journal of Cell Biology 105:2123–2135.